

Article

New Approach of Normal and Shear Stress Components for Multiple Curvilinear Holes Which Weakened a Flexible Plate

Faizah M. Alharbi * and Nafeesa G. Alhendi

Mathematics Department, Faculty of Sciences, Umm Al-Qura University, Makkah 24227, Saudi Arabia; nghendi@uqu.edu.sa

* Correspondence: fmharbi@uqu.edu.sa

Abstract: In this article, a thin infinite flexible plate weakened by multiple curvilinear holes is considered. The strength shapes are mapped outside a unit circle with the assistance of particular conformal mapping under certain conditions. The mathematical model that governs the rounded forces of the current physical problem is the boundary value problem of elastic media. This study is applicable to many phenomena throughout nature, like tunnels, caves, and excavations in soil or rock. The Cauchy method for complex variables is used to get the closed forms of Goursat functions and change the problem to a second-type integrodifferential equation with a Cauchy kernel, which is used for a large area of the contact problems. Then, the normal and shear stress components that act on the model are derived. Afterward, some of the physical applications are studied, and different stress components at specific values in each application are calculated and plotted using Maple 2023.

Keywords: complex variables method; Goursat functions; conformal mapping; first and second fundamental problem; normal and shear stresses



Citation: Alharbi, F.M.; Alhendi, N.G. New Approach of Normal and Shear Stress Components for Multiple Curvilinear Holes Which Weakened a Flexible Plate. *Symmetry* **2024**, *16*, 360. <https://doi.org/10.3390/sym16030360>

Academic Editor: Christos Volos

Received: 7 February 2024

Revised: 12 March 2024

Accepted: 14 March 2024

Published: 16 March 2024



Copyright: © 2024 by the authors. Licensee MDPI, Basel, Switzerland. This article is an open access article distributed under the terms and conditions of the Creative Commons Attribution (CC BY) license (<https://creativecommons.org/licenses/by/4.0/>).

1. Introduction

There is often more stress concentrated in the vicinity of holes in plate structural components when external loads are applied. To assess the stability and strengthening of the structure, it is crucial to compute the stresses on the edges of the holes precisely. Odishelidze and Criado-Aldeanueva [1] studied axially symmetric problems of the plane theory of elasticity with partially unknown limits, where these problems were studied for a rhombus weakened by one or two holes. Manickam et al. [2] attempted to study the nonlinear thermo-elastic buckling characteristics of composite variable stiffness beams with layers using curvilinear fibers under a thermal environment. Hsieh and Hwu [3] derived a full-field solution for an infinite anisotropic plate containing a hole perturbed from an ellipse subjected to uniform loading at infinity with Stroh formalism. Kaloerov et al. [4] presented a general solution to the problems of elasticity theory for anisotropic half-planes and strips with arbitrary holes and cracks. Li et al. [5] presented a modified Laurent series to investigate the elastic field around holes and inclusions under plane deformation. Akinola [6] emphasized the alternate formulation of the Cauchy–Riemann criteria for the analyticity of a complex variable function. Using the complex variable method, Guo and Lu [7] proposed a new approach to solving the elastic–plastic fields close to the elliptical hole’s major-axis line. Ioakimidis and Theocaris [8] suggested a numerical approach for the solution of Cauchy-type singular integral equations along contours in the complex plane. Strack and Verruijt [9] derived an analytical solution for an energetic tunnel in a flexible half-plane. The half-plane’s surface is stress-free, and the tunnel experiences a defined displacement within its circumference. Li and Fan [10] developed the complex variable technique for the plane elasticity theory of icosahedral quasi-crystals. Yu et al. [11] investigated the linear piezoelectric behavior of one-dimensional (1D) hexagonal quasicrystals using the symmetry operations of point groups. Jiao et al. [12] investigated the Reddy-proposed dual mesh control domain method (DMCDM), which combines the benefits of the finite

element approach (variable interpolation) and the finite volume method (a global form of the fulfillment of the governing equations).

Identifying $\chi_1(r)$ and $\varpi_1(r)$, two analytic functions of a single complex input $z = x + iy$, is known to be the equivalent (see [13]) of solving the first and second boundary value problems. These functions have to satisfy the following boundary conditions:

$$L\chi_1(r) - r\overline{\chi_1'(r)} - r\overline{\varpi_1(r)} = g(r), \quad (1)$$

where $g(r)$ is a predefined function of stresses for the first boundary value problem with $L = -1$. For the second boundary value problem, $g(r)$ is a known function of displacement. If $|\tau| > 1$, then the area outside of a closed contour that is infinite can be conformally mapped outside of the unit circle. This concerns the rational mapping function $z = c\zeta(\tau)$, where $c > 0$ and $\varpi'(\tau)$ do not go away or become infinite. Both $\chi_1(r)$ and $\varpi_1(r)$ are complex potential functions of the following forms (see [14]):

$$\mathcal{O}_1(z) = -\frac{S_x + iS_y}{2\pi(1+k)} \ln \tau + c\Gamma\tau + \chi(\tau), \quad (2)$$

and

$$\mathcal{S}_1(z) = \frac{k(S_x - iS_y)}{2\pi(1+k)} \ln \tau + c\Gamma^+\tau + \varpi(\tau). \quad (3)$$

Several authors, including [14–16], have discussed the boundary problems for holed infinite plates. A few of them described the solutions as power series using the Laurent theorem. Another technique for dealing with complex variables is the application of Goursat functions. They take advantage of the characteristics of the circle or any mapped region of Cauchy integrals outside of a unit circle by using the general rational mapping function $z = c\zeta(\tau)$. They obtain a solution in the form of two complex functions. Abdou et al. [15] applied the Goursat functions in the complex variable approach to deduce the first and second types on a limitless plate with two holes that curve. Abdou and Monaqueul [17] solved the fundamental problems of an infinite plate with a hole that is weakened by a strong pole in any form using the Cauchy singular technique. Mattei and Lim [18] defined a density basis function on the inclusion's border using the coordinate system made available by the exterior conformal mapping of the inclusion. To create a closed form of Goursat functions with variant time, Alhazmi et al. [19] used the complex variables approach and assumed an infinite elastic plate that had two holes weakening it. Leonhardt [20] created a generic formula for designing media that produces perfect invisibility while maintaining geometrical optic precision. Trefethen [21] developed new methods for numerical conformal mapping based on the least-squares fitting on the boundary and rational approximations for solving Dirichlet problems. Caprini [22] discussed a reformulation of QCD perturbation theory as an expansion in terms of a set of nonpower functions of the strong coupling. Kiosak et al. [23] have investigated the conformal mappings of particular quasi-Einstein spaces. Symm [24] presented an integral equation technique for determining the conformal mapping of a given simply connected domain onto the unit circle's interior. O'Donnell and Rokhlin [25] presented a method for creating conformal mappings from any simply linked region in the complex plane onto the unit disk. Fu et al. [26] obtained the equivalent invariant under a class of conformal mappings between two semi-Riemannian manifolds. Moreover, Ghods et al. [27] applied conformal mapping to create the permeance network for complex-geometry air-gap regions. Mukherjee and Fok [28] presented a novel method for computing the fiber field in a generic artery cross-section by applying conformal maps. The technique relies on finding a rational approximation of the conformal map. Wu et al. [29] proposed a numerical method for the conformal mapping of closed-box girder bridges and applied it to flutter performance prediction, which is crucial for ensuring the safety and sustainability of bridge structures.

In this work, we consider a thin infinite flexible plate with a thickness h weakened by multiple curvilinear holes. The plate is subject to external stress that acts in all directions

(see Figure 1). If we ignore any effects related to the physical media surrounding the plate, like temperature, dryness, viscosity, etc., we assume that the stress forces are distributed evenly over the area of the plate, except at the holes. These holes are the important regions of the current study and take different shapes; each one has a physical meaning and a different intensity of effect from the stress forces. The current approach in this work is to reduce the area of energy dissipation, the hole regions, to a finite uniform domain. To accomplish this, we use conformal mapping, which does not vanish or become infinite outside a unit circle. The technique's idea is to transfer the complex plane, which has curvilinear holes. To achieve this, we use a specific conformal mapping. The conformal mapping technique is tailored to this problem in two dimensions. An algorithm is introduced to compute the conformal map for the chosen boundaries to simply study shapes from the conformal map. We apply the complex variables method with the Cauchy technique to solve the boundary value problem and obtain a closed form of the Goursat functions. Then, the problem is reduced to the integrodifferential equation of the second type with a Cauchy kernel. Moreover, the normal and shear stress components are derived. After that, we explain different physical applications, and then the normal and shear stress components for each one at the chosen values are calculated and plotted using the Maple 2023 software. Finally, the main results of the work are discussed.

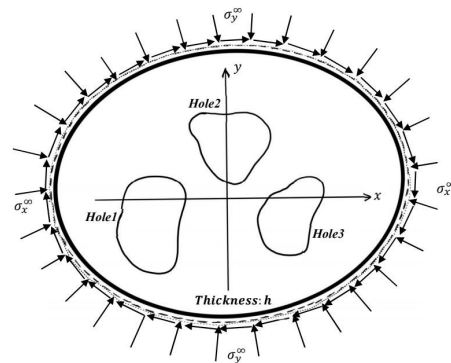


Figure 1. Three different holes in an infinite plate.

2. Basic Equations

In the given area, the boundary S is in the z -plane and is occupied by the plate's center plane. This boundary is mapped onto the unit circle δ in the τ -plane by the rational mapping $z = c\zeta(\tau)$. Using the formula $\tau = \rho e^{i\theta}$, curvilinear coordinates (ρ, θ) are introduced as maps of the polar conditions into the z -plane. The following result is obtained when we apply $z = c\zeta(\tau)$ to (1):

$$L\chi_1(c\zeta(\tau)) - \frac{\zeta(\tau)}{\zeta'(\tau)}\chi_1(c\zeta(\tau)) - \omega_1(c\zeta(\tau)) = g(c\zeta(\tau)). \quad (4)$$

In the τ -plane, the first and second boundary value problems are represented by Formula (4). The related formulas of (1) are as follows:

$$\chi_1(r) + r\overline{\chi_1'(r)} + \overline{\omega_1(r)} = \frac{1}{2G} \int_0^s [iY(s) - Z(s)] ds + c, \quad (5)$$

$$k\chi_1(r) - r\overline{\chi_1'(r)} - \overline{\omega_1(r)} = p + iq, \quad (6)$$

where the applied stresses, denoted as $Y(s)$ and $Z(s)$, are defined on the edge of the plane; the displacement variables are p and q , the length is s , and the modulus of shear is G . In addition, the following conditions must be fulfilled by the applied stresses $Y(s)$ and $Z(s)$:

$$Y(s) = \sigma_{xx} \frac{dy}{ds} - \sigma_{xy} \frac{dx}{ds}, \quad (7)$$

$$Z(s) = \sigma_{yx} \frac{dy}{ds} - \sigma_{yy} \frac{dx}{ds}. \quad (8)$$

In elastic problems of the plate, the stress components are given by

$$\begin{aligned} \sigma_{xx} - \sigma_{yy} + 2i\sigma_{xy} &= -4G \left[z\overline{\chi''(z)} + \overline{\varpi'(z)} \right], \\ \sigma_{xx} + \sigma_{yy} &= 4G \left[\chi'(z) + \overline{\chi'(z)} \right]. \end{aligned} \quad (9)$$

3. Conformal Mapping and Special Cases

We consider an infinitely thin plate with a curvilinear hole S whose origin is outside the unit circle δ in the τ -plane ($\tau = \rho e^{i\theta}$, $0 \leq \theta \leq 2\pi$) with a rational mapping function

$$z = c\zeta(\tau) = c \frac{\tau + \sum_{i=1}^3 m_i \tau^{-il}}{\prod_{i=1}^3 (1 - n_i \tau^{-l})}, \quad (10)$$

where $z'(\tau)$ does not become infinite or vanish, m_i are complex numbers, and n_i are real numbers.

The study focused on normal and shear stress components for flexible plates, which were weakened by curvilinear holes conformally mapped on the domain outside a unit circle by the rational function (10). The physical interest of mapping comes from the different shapes of holes it treats, as shown in Figures 2–13.

Special Cases:

- When $|n_i| < 1$, the mapping represents a skew-symmetric simple closed curve. See Figures 2–5.
- When $|n_i| > 1$, the mapping reduces to $(i + 1)$ crossed curves. So, the curvilinear holes degenerate into multiple closed curves and have strong poles. See Figures 6–9.
- At the values of n in Figures 10–13, the curvilinear holes generated two skew-symmetric poles around the x-axis.

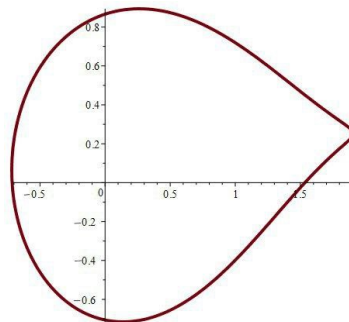


Figure 2. $m_1 = -0.3 + i$, $m_2 = -0.2 - i$, $m_3 = 0.3 + i$, $n_1 = -0.2$, $n_2 = 0.3$, $n_3 = 0.4$.

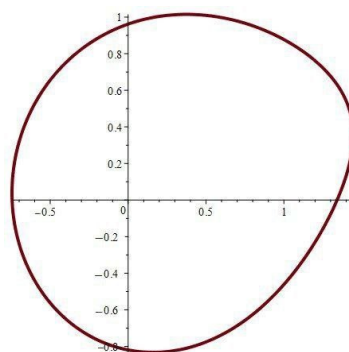


Figure 3. $m_1 = -2 + i$, $m_2 = -1 - i$, $m_3 = 4 + i$, $n_1 = 0.1$, $n_2 = 0.2$, $n_3 = 0.3$.

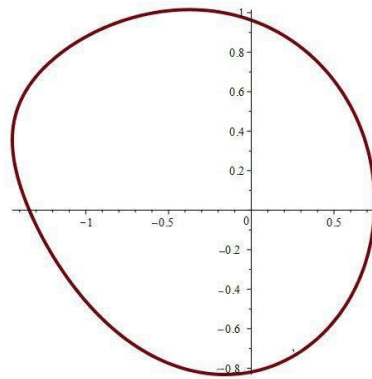


Figure 4. $m_1 = 2 + i, m_2 = 1 - i, m_3 = -4 + i, n_1 = -0.1, n_2 = -0.2, n_3 = -0.3$.

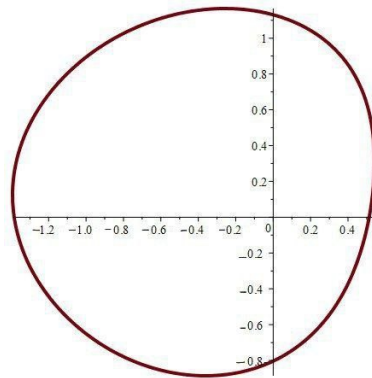


Figure 5. $m_1 = -5 + i, m_2 = 4 + i, m_3 = 4 - i, n_1 = 0.1, n_2 = -0.2, n_3 = 0.3$.

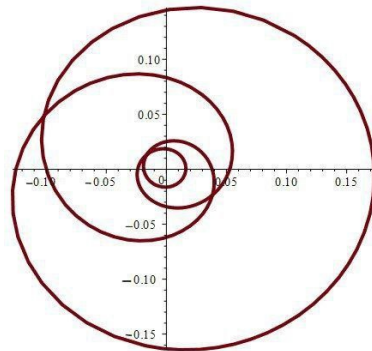


Figure 6. $m_1 = -0.2 + i, m_2 = -0.3 + i, m_3 = 0.4 + i, n_1 = -2, n_2 = -3, n_3 = -4$.

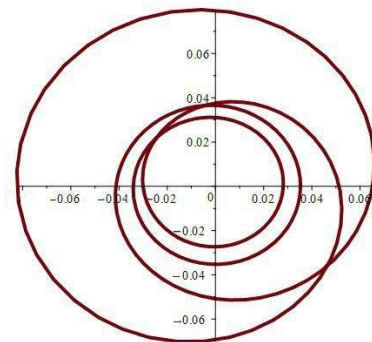


Figure 7. $m_1 = 0.1 + i, m_2 = 0.3 + i, m_3 = -0.5 + i, n_1 = -2, n_2 = 3, n_3 = -4$.

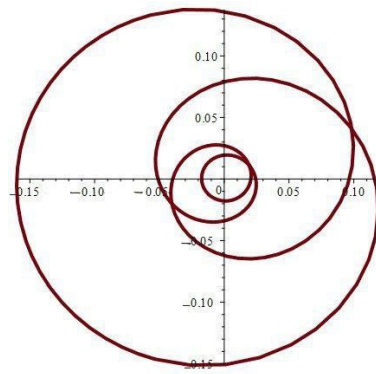


Figure 8. $m_1 = -0.3 + i, m_2 = -0.2 - i, m_3 = 0.3 + i, n_1 = 2, n_2 = 3, n_3 = 4$.

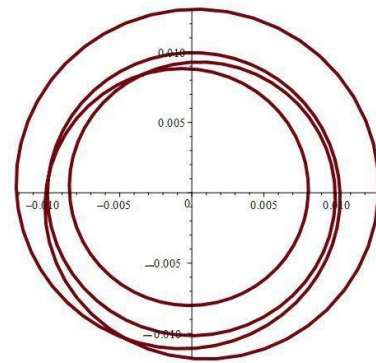


Figure 9. $m_1 = -0.3 + i, m_2 = -0.2 - i, m_3 = 0.3 + i, n_1 = 2\sqrt{2}, n_2 = -3.5, n_3 = 10$.

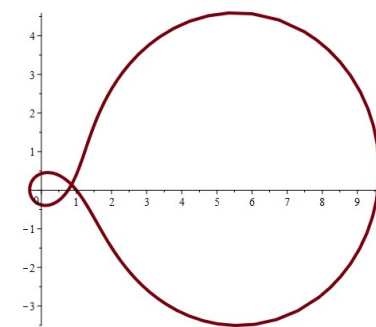


Figure 10. $m_1 = -0.3 + i, m_2 = -0.2 - i, m_3 = 0.3 + i, n_1 = 0.2, n_2 = 0.5, n_3 = 0.75$.

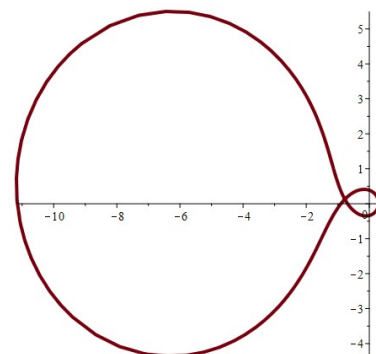


Figure 11. $m_1 = -0.3 + i, m_2 = -0.2 - i, m_3 = 0.3 + i, n_1 = -0.25, n_2 = -0.5, n_3 = -0.75$.

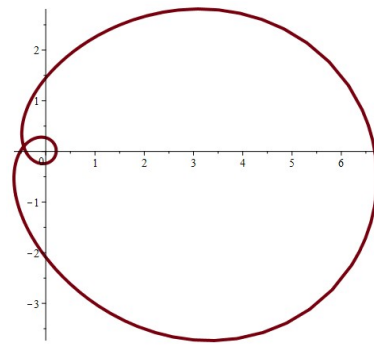


Figure 12. $m_1 = -0.3 + i, m_2 = -0.2 - i, m_3 = 0.3 + i, n_1 = -\sqrt{2}, n_2 = -0.5, n_3 = -0.25$.

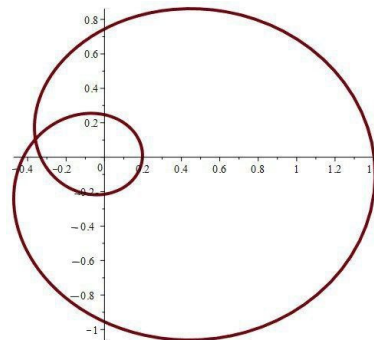


Figure 13. $m_1 = -0.3 + i, m_2 = -0.2 - i, m_3 = 0.3 + i, n_1 = -0.2, n_2 = -\sqrt{5}n_3 = -0.25$.

4. The Method of Solution

The complex Goursat functions, $\chi(\tau)$ and $\omega(\tau)$, are derived using the complex variable technique (see [30,31]). Furthermore, after determining the Goursat functions, the three stress components, σ_{xx} , σ_{xy} , and σ_{yy} , will be completely determined. With the boundary condition (1) and the conformal mapping (4), the expression $\zeta(\tau)/\zeta'(\tau^{-1})$ yields

$$\frac{\zeta(\tau)}{\zeta'(\tau^{-1})} = \alpha(\tau) + \beta(\tau^{-1}), \tag{11}$$

where $\beta(\tau)$ is a regular function, and

$$\alpha(\tau) = \frac{h_1}{\tau - n_1} + \frac{h_2}{\tau - n_2} + \frac{h_3}{\tau - n_3}, \tag{12}$$

with

$$h_j =: \frac{Q}{R},$$

where

$$Q = [n_j^{v+2} + m_1 n_j^{v+1} + m_2 n_j + m_3] (1 - n_j^2) (1 - n_1 n_2)^2 (1 - n_1 n_3)^2 (1 - n_2 n_3)^2,$$

$$R = (n_j - n_{\pm 1}) \times \left[(1 - n_j^2) (1 - n_1 n_2) (1 - n_1 n_3) (1 - n_2 n_3) \gamma_j^{(1)} - \ln \gamma_j^{(2)} (n_1 + n_2 + n_3 - 2n_j n_{j+1}) \right],$$

$$\gamma_j^{(2)} = 1 + m_1 n_j^v + m_2 n_j^{v+1} + m_3 n_j^{v+2}, \tag{13}$$

for $j = 1, 2, 3$, and $|\tau| > 1$. By virtue of (2), (3), and (11), the condition at the boundary (4) is

$$k\chi(\sigma) - \alpha(\sigma)\overline{\chi'(\sigma)} - \overline{\omega_*(\sigma)} = g_*(\sigma), \tag{14}$$

where $\sigma = e^{i\theta}$ denotes the value on the edge of the unit circle,

$$\omega_*(\tau) = \omega(\tau) + \beta(\tau)\chi'(\tau),$$

and

$$g_*(\tau) = F(\tau) - ckl^{-1}\tau + c\overline{\Gamma^*}\tau^{-1} + N(\tau)[\alpha(\tau) + \overline{\beta(\tau)}],$$

with

$$N(\tau) = c\overline{\Gamma} - \frac{S_x - iS_y}{2\pi(1+k)}\tau,$$

and

$$F(\tau) = g(r) = g(c\zeta(\tau)).$$

The Hölder condition (see [32]) is thought to be satisfied by the function $g(\sigma)$ and its derivatives. Our aim is to use the mapping $z = c\frac{\tau+m\tau^{-1}}{1-n\tau^{-1}}$ to obtain the functions $\chi(\zeta)$ and $\omega(\zeta)$ for various boundary value problems. To achieve this, we multiply both sides of this mapping by $\frac{d\sigma}{2\pi i(\sigma-\tau)}$. Then, we integrate the resulting integrals using residue theorems. Thus, we obtain

$$L\chi(\tau) + \frac{1}{2\pi i} \int_{\gamma} \frac{\alpha(\sigma)\overline{\chi'(\sigma)}}{\sigma-\tau} d\sigma = c\overline{\Gamma^*}\tau^{-1} + A(\tau) + \frac{h_1}{\tau-n_1^{\nu-1}}N(n_1^{\omega-1}) + \frac{h_2}{\tau-n_2^{\nu-1}}N(n_2^{\omega-1}) + \frac{h_3}{\tau-n_3^{\nu-1}}N(n_3^{\omega-1}), \tag{15}$$

where

$$\nu = 1 + \frac{1}{l},$$

and

$$A(\tau) = \frac{1}{2\pi i} \sum_{\eta=0}^{\infty} \tau^{-\eta-1} \int_{\delta} \sigma^{\eta} F(\sigma) d\sigma. \tag{16}$$

Using (11) in the integral term of (15), we assume

$$\frac{1}{2\pi i} \int_{\delta} \frac{\alpha(\sigma)\overline{\chi'(\sigma)}}{\sigma-\tau} d\sigma = \frac{ch_1b_1}{n_1^{\nu-1}-\tau} + \frac{ch_2b_2}{n_2^{\nu-1}-\tau} + \frac{ch_3b_3}{n_3^{\nu-1}-\tau}, \tag{17}$$

where the complex constants b_j 's are yet to be found. Therefore, we have

$$-L\chi(\tau) = A(\tau) - c\overline{\Gamma^*}\tau^{-1} = \sum_{j=1}^3 \frac{h_j \left(cb_j + N(n_j^{\nu-1}) \right)}{h_j^{\nu-1} - \tau}. \tag{18}$$

Differentiating (18) with respect to τ and using the $\chi'(\sigma)$ result from (17), we obtain

$$cLb_j + cn_j^2\overline{\Gamma^*} + d_jh_j \left[\overline{cb_j} + \overline{N(n_j^{\nu-1})} \right] = -\overline{A'(n_j)}, \text{ for } j = 1, 2, 3. \tag{19}$$

The general solution of (19) is

$$b_j = \frac{KE_j - h_jd_j\overline{E_j}}{c(K^2 - h_j^2d_j^2)},$$

where

$$E_j = -\overline{A'(n_j)} - c\Gamma^* n_j^{2(v-1)} - h_j d_j N(n_j^{v-1}),$$

and

$$d_j = n_j^{2(v-1)} \left(1 - n_1^{v-1} n_2^{v-1} n_3^{v-1}\right)^{-2} \overline{N(n_j^{v-1})}. \quad (20)$$

From the boundary condition (14), $\omega(\tau)$ can be determined in the form

$$\begin{aligned} \omega(\tau) = & \frac{cL\bar{\Gamma}}{\tau} - \frac{\bar{\xi}(\tau)}{\bar{\xi}'(\tau^{-1})} \chi_*(\tau) + \frac{h_1 \tau}{1 - n_1^{v-1} \tau} \chi_*(n_1^{\xi-1}) + \frac{h_2 \tau}{1 - n_2^{v-1} \tau} \chi_*(n_2^{\xi-1}) \\ & + \frac{h_3 \tau}{1 - n_3^{v-1} \tau} \chi_*(n_3^{\xi-1}) + B(\tau) - B, \end{aligned} \quad (21)$$

where

$$\chi_*(\tau) = \chi'(\tau) + \overline{N(\tau)},$$

$$B(\tau) = \frac{1}{2\pi i} \int_{\delta} \frac{F(\sigma)}{\sigma - \tau} d\sigma,$$

and

$$B = \frac{1}{2\pi i} \int_{\delta} \frac{\overline{F(\sigma)}}{\sigma - \tau} d\sigma. \quad (22)$$

Using (18) in (9), after some derivatives and algebraic relations, we have

$$\begin{aligned} \sigma_{xx} &= 2G[-\delta(z^2 + 4z\bar{z} + \bar{z}^2) \operatorname{Im} z + \operatorname{Re}(2\chi'(\tau) - M(\tau, \bar{\tau}))], \\ \sigma_{yy} &= 2G[\delta(z^2 + \bar{z}^2) \operatorname{Im} z + \operatorname{Re}(2\chi'(\tau) + M(\tau, \bar{\tau}))], \\ \sigma_{xy} &= 2G[\delta(z\bar{z} - 2(\operatorname{Im} z)^2 \operatorname{Re} z + \operatorname{Im} M(\tau, \bar{\tau}))], \end{aligned} \quad (23)$$

where

$$\begin{aligned} M(\tau, \bar{\tau}) = & \left[c(\tau) - \frac{\bar{\xi}(\tau)}{\bar{\xi}'(\tau)} \right] \overline{\chi''(\tau)} + \frac{S_x - is_y}{2\pi(1+k)} \frac{\bar{\xi}(\tau)}{\bar{\xi}'(\tau)} + ck\Gamma\tau^2 \\ & - \frac{\bar{\xi}(\tau)}{\bar{\xi}'(\tau)} \left[\overline{\chi'(\tau)} + N(\tau) \right] + \overline{B'(\tau)} + \sum_{i=1}^3 \frac{h_i \tau}{(\tau - n_i^{v-1})^2} \chi_*(n_i^{v-1}), \end{aligned}$$

and

$$\delta = \frac{(1+\nu)r_0^2}{2(z\bar{z})^2}. \quad (24)$$

5. Applications

In this section, we resolve the first and second boundary value problems by assuming various values for the given functions. In this case, the Goursat functions will then be obtained, allowing for the direct calculation of the stress components.

Application 1: A curvilinear hole with uniform tensile stress on an infinite plate: There is an applied uniform tensile tension of intensity P to an infinite plate, stretching it to infinity and forming an angle θ with the x -axis in the given conditions: $L = -1$, $\Gamma^* = \frac{P}{4}$, $\Gamma^* = \frac{-P}{2} e^{-2i\theta}$, $0 \leq \theta \leq 2\pi$, and $S_x = S_y = g = 0$. The two complex functions of (19) and (21) result in the plate becoming weaker due to a curvilinear hole S that is not under any stress:

$$\chi(\tau) = \frac{cp}{2} e^{2i\theta} \tau^{-1} + \sum_{j=1}^3 \frac{L_j^{(1)}}{n_j^{v-1} - \tau}, \quad (25)$$

$$\omega(\tau) = \frac{-cp}{2} \tau^{-1} - \frac{\bar{\xi}(\tau^{-1})}{\bar{\xi}'(\eta)} \chi_*(\tau) + \sum_{j=1}^3 \frac{h_j \tau}{1 - n_j^{v-1} \tau} \chi_*(n_j^{\xi-1}), \quad (26)$$

where

$$L_j^{(1)} = \frac{Ph_i}{4} \left[\frac{1 - 2n_j^{2(v-1)} \cos 2\theta}{1 - h_j d_j} + \frac{2n_j^{2(v-1)} \sin 2\theta}{1 + h_j d_j} \right],$$

and

$$\chi_*(\tau) = \chi'(\tau) + \frac{cp}{4}.$$

Using (25) and (26) in (23), it is possible to obtain the stress components $\sigma_{xx}, \sigma_{yy}, \sigma_{xy}$ directly. Figures 14–19 show the equations that relate these stress components to the angle θ .

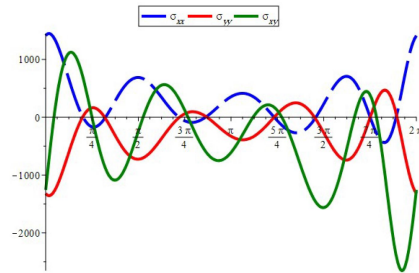


Figure 14. The relation between stress components and the angle θ .

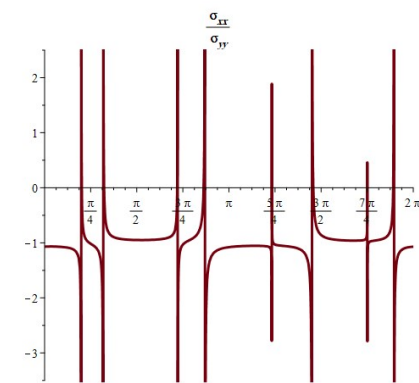


Figure 15. Stress ratio where $n_1 = 2, n_2 = 3, n_3 = 4$.

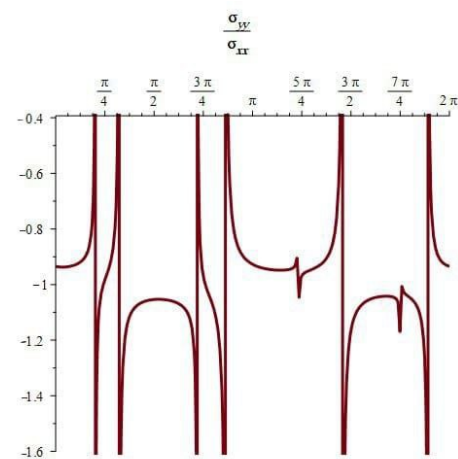


Figure 16. Stress ratio where $n_1 = 2, n_2 = 3, n_3 = 4$.

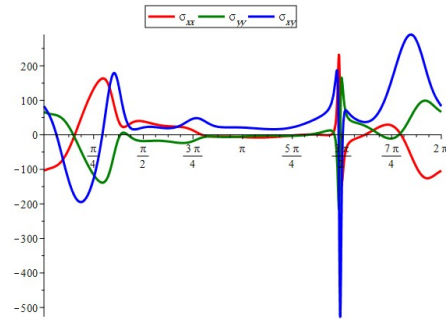


Figure 17. The relation between stress components and the angle θ .

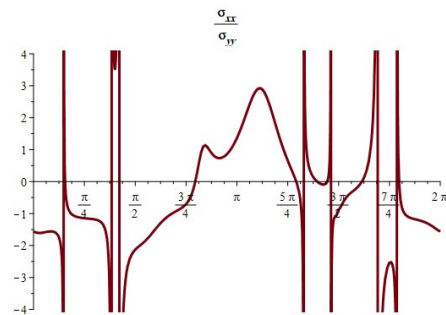


Figure 18. Stress ratio where $n_1 = 0.3, n_2 = 0.25, n_3 = 0.4$.

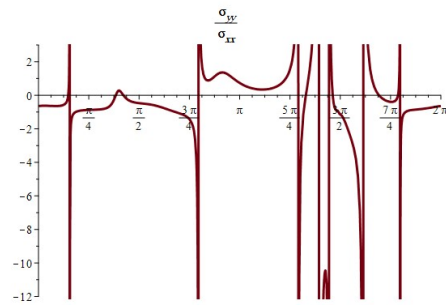


Figure 19. Stress ratio where $n_1 = 0.3, n_2 = 0.25, n_3 = 0.4$.

Application 2: A two-pole curvilinear hole with a uniformly pressured edge: In the case of $L = -1, S_x = S_y = \Gamma = \Gamma^* = 0$, and $g(f(r)) = Pr$, where P is a real constant, the Equations (19) and (21) become

$$\begin{aligned} \chi(\tau) = & \frac{cP(n_1^{1+\nu} + m_1n_1 + m_2)}{(n_1^{\nu-1} - \tau)(1 - h_1d_1)(n_1 - n_2)} + \frac{cP(n_2^{1+\nu} + m_2n_2 + m_1)}{(n_2^{\nu-1} - \tau)(1 - h_2d_2)(n_2 - n_1)} \\ & + \frac{cP(n_2^{1+\nu} + m_2n_2 + m_3)}{(n_2^{\nu-1} - \tau)(1 - h_2d_2)(n_2 - n_3)} + \frac{cP(n_1^{1+\nu} + m_1n_1 + m_3)}{(n_1^{\nu-1} - \tau)(1 - h_1d_1)(n_1 - n_3)} \\ & + \frac{cP(n_3^{1+\nu} + m_3n_3 + m_1)}{(n_3^{\nu-1} - \tau)(1 - h_3d_3)(n_3 - n_1)} + \frac{cP(n_3^{1+\nu} + m_3n_3 + m_2)}{(n_3^{\nu-1} - \tau)(1 - h_3d_3)(n_3 - n_2)}, \end{aligned} \tag{27}$$

$$\begin{aligned} \omega(\tau) = & -cP(n_1 + n_2 + n_3 + \tau^{-1}) - \frac{\xi(\tau^{-1})}{\xi'(\tau)}\chi'(\tau) + \frac{h_1\tau}{1 - n_1^{\nu-1}\tau}\chi^*(n_1^{\nu-1}) \\ & + \frac{h_2\tau}{1 - n_2^{\nu-1}\tau}\chi^*(n_2^{\nu-1}) + \frac{h_3\tau}{1 - n_3^{\nu-1}\tau}\chi^*(n_3^{\nu-1}). \end{aligned} \tag{28}$$

Hence, when a constant pressure of P is applied to the hole's edge, Equations (27) and (28) provide the solution to the first boundary value problem. On the other hand, when the edge is under a uniform tangential stress of T , as stated in (27) and (28), we replace P with iT in (27) and (28).

Figures 20–25 show the equations relating the stress components to the angle θ .

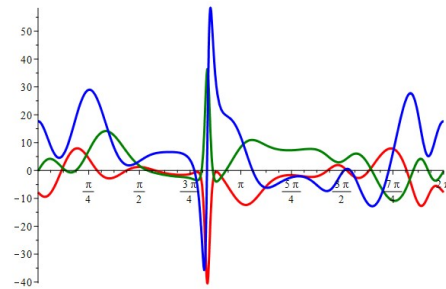


Figure 20. The relation between stress components and the angle θ .

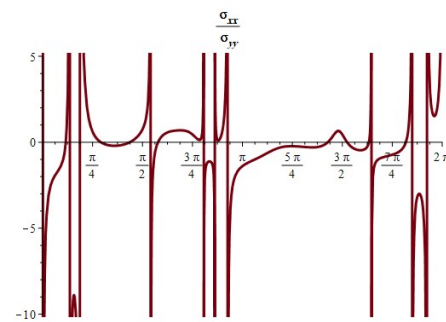


Figure 21. Stress ratio where $n_1 = 0.2, n_2 = 0.3, n_3 = -0.4$.

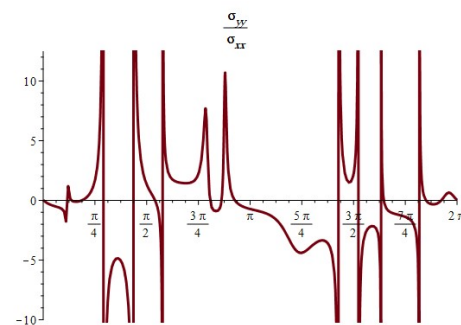


Figure 22. Stress ratio where $n_1 = 0.2, n_2 = 0.3, n_3 = -0.4$.

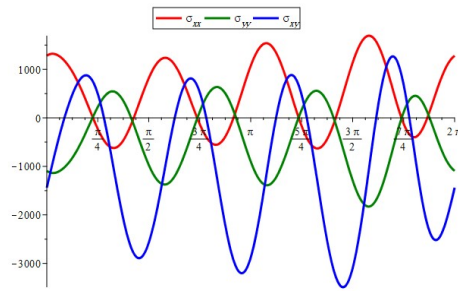


Figure 23. The relation between stress components and the angle θ .

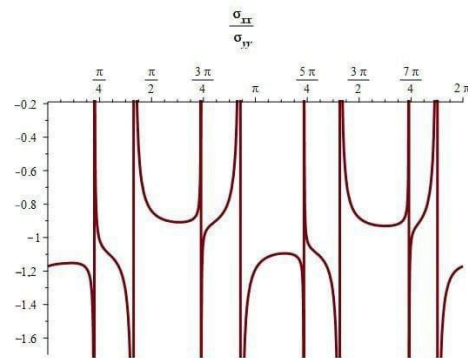


Figure 24. Stress ratio where $n_1 = 5, n_2 = 4, n_3 = -7$.

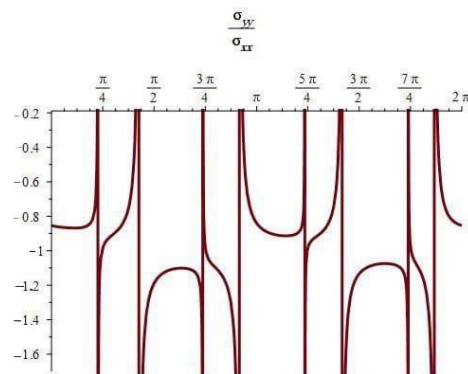


Figure 25. Stress ratio where $n_1 = 5, n_2 = 4, n_3 = -7$.

Application 3: The curvilinear hole’s center is where the force acts. We assume that the strains, in this case, finish at infinity. The kernel’s lack of rotation is immediately apparent. The kernel usually stays in its original location. Consequently, the Goursat functions are determined by assuming that $\Gamma = \Gamma^* = f(t) = 0$ and $L = k$. Thus,

$$\begin{aligned}
 -k\chi(\tau) = \frac{c}{2\pi(1+k)} \sum_{j=1}^3 \frac{h_j n_j}{n_j^{v-1} - \tau} \left[\frac{kh_j d_j (S_x - iS_y)}{c(k^2 - h_j^2 d_j^2)} \right. \\
 \left. - \left(1 + \frac{h_j d_j^2}{c(k^2 - h_j^2 d_j^2)} \right) (S_x - iS_y) \right], \tag{29}
 \end{aligned}$$

and

$$\chi_*(\tau) = \frac{h_1\tau}{1-n_1^{\nu-1}\tau}\chi_*(n_1^{1-\nu}) + \frac{h_2\tau}{1-n_2^{\nu-1}\tau}\chi_*(n_2^{1-\nu}) + \frac{h_3\tau}{1-n_3^{\nu-1}\tau}\chi_*(n_3^{1-\nu}) - \frac{\xi(\gamma^{-1})}{\xi'(\tau)}\chi_*(\tau), \tag{30}$$

where

$$\chi_*(\tau) = \chi'(\tau) - \frac{S_x + iS_y}{2\pi(1+k)\tau}.$$

As a result, the second boundary value problem is resolved, where the curvilinear kernel's center is subject to a force (S_x, S_y) .

The equations relating the stress components to the angle θ are shown in Figures 26–31.

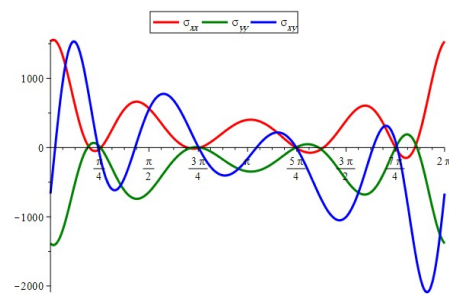


Figure 26. The relation between stress components and the angle θ .

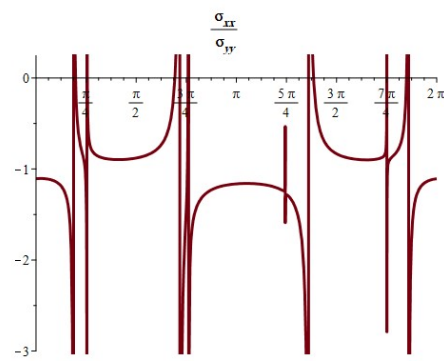


Figure 27. Stress ratio where $n_1 = 3, n_2 = 5, n_3 = 4$.

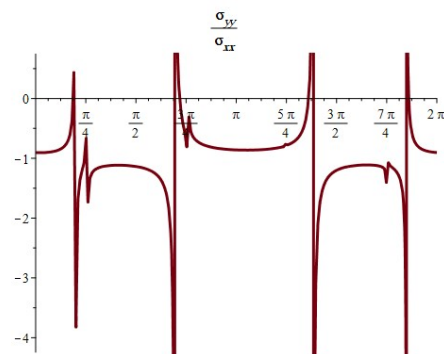


Figure 28. Stress ratio where $n_1 = 3, n_2 = 5, n_3 = 4$.

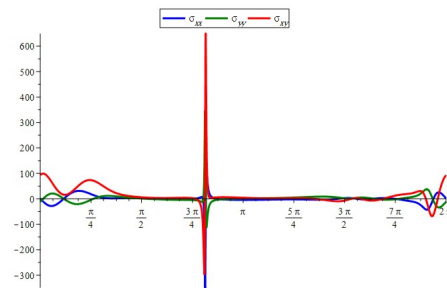


Figure 29. The relation between stress components and the angle θ .

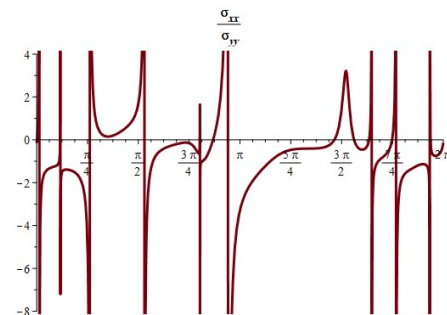


Figure 30. Stress ratio where $n_1 = 0.2, n_2 = 0.3, n_3 = 0.5$.

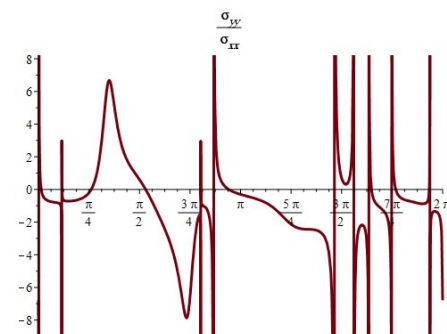


Figure 31. Stress ratio where $n_1 = 0.2, n_2 = 0.3, n_3 = 0.5$.

6. Conclusions

In this work, we examined a thin infinite flexible plate with a thickness h weakened by multiple curvilinear holes. There was external stress acting in all directions on the plate. The stress forces are distributed uniformly throughout the plate, except for the edges of the holes, and we disregarded any effects associated with the physical medium surrounding the plate. These holes, which were the focal point of the present investigation, came in various forms, and each had a distinct physical significance and a varying degree of stress force impact. The area of energy dissipation, or the hole area, was reduced to a limited uniform domain using the present methodology; we achieved this by using a certain conformal mapping $z = c\zeta(\tau)$, where $c > 0$ to provide the solution to the boundary value problem as a discontinuous kernel integrodifferential equation. This kind of integrodifferential equation plays a famous role in many important applications of contact problems in elastic media and material engineering sciences; see [33–35]. The Cauchy technique is a powerful tool that allows us to simplify the singular or super-strong singular problem, enabling us to handle it more efficiently. After obtaining the two Goursat functions, $\chi(\tau)$, $\omega(\tau)$, the components of normal and shear stress were determined. The theoretical knowledge is explained, applicably, by the chosen applications in Section 5, as follows:

- When $|n_i| > 1$, the component of the stress acts as a tensile force. The normal and shear stress component take the shapes of nonhomogeneous waves and form an angle with the x-axis; see Figures 14, 23 and 26. Furthermore, the stress ratio $\frac{\sigma_{xx}}{\sigma_{yy}}$ and $\left(\frac{\sigma_{xx}}{\sigma_{yy}}\right)^{-1}$ represents the uniform oscillation; see Figures 15, 16, 24, 25, 27 and 28.
- When $|n_i| < 1$, the component of the stress acts as a compression force. The normal and shear stress component take the shapes of compressed interfering waves and form an angle with the x-axis; see Figures 17, 20 and 29. Furthermore, the stress ratio $\frac{\sigma_{xx}}{\sigma_{yy}}$ and $\left(\frac{\sigma_{xx}}{\sigma_{yy}}\right)^{-1}$ represents a compressed oscillation; see Figures 18, 19, 21, 22, 30 and 31.

Future Work:

1. Study the physical model when the complex potential functions are functions of time. Also, study it in the presence of external forces like flowing heat or a normal magnetic field.
2. Study the anomaly model as an application in the medical field. For example, osteoporosis is characterized by a reduction in bone tissue volume and thickness. This causes the bones to weaken and break more easily. Another example is sickle cell anemia, an inherited condition in which red blood cells have an irregular crescent shape, block small blood vessels, and live a shorter life than normal red blood cells.

Author Contributions: Conceptualization, F.M.A.; Methodology, F.M.A. and N.G.A.; Software, N.G.A.; Validation, N.G.A.; Writing—original draft, N.G.A.; Writing—review & editing, N.G.A.; Supervision, F.M.A.; Project administration, F.M.A.; Funding acquisition, F.M.A. All authors have read and agreed to the published version of the manuscript.

Funding: This research received no external funding.

Data Availability Statement: Data are contained within the article.

Conflicts of Interest: The authors declare that they have no conflicts of interest.

References

1. Odishelidze, N.; Criado-Aldeanueva, F. Some axially symmetric problems of the theory of plane elasticity with partially unknown boundaries. *Acta Mech.* **2008**, *199*, 227–240. [\[CrossRef\]](#)
2. Manickam, G.; Haboussi, M.; D’Ottavio, M.; Kulkarni, V.; Chettiar, A.; Gunasekaran, V. Nonlinear thermo-elastic stability of variable stiffness curvilinear fibres based layered composite beams by shear deformable trigonometric beam model coupled with modified constitutive equations. *Int. J. Non-Linear Mech.* **2023**, *148*, 104303. [\[CrossRef\]](#)
3. Hsieh, M.-L.; Hwu, C. A full field solution for an anisotropic elastic plate with a hole perturbed from an ellipse. *Eur. J. Mech. A Solids* **2023**, *97*, 104823. [\[CrossRef\]](#)
4. Kaloerov, S.; Glushankov, E.; Mironenko, A. Solution of problems of elasticity theory for multiply connected half-planes and strips. *Mech. Solids* **2023**, *58*, 1063–1075. [\[CrossRef\]](#)
5. Li, C.; Huang, C.; Wang, S.; Cai, D. A modified laurent series for hole/inclusion problems in plane elasticity. *Z. Angew. Math. Phys.* **2021**, *72*, 124. [\[CrossRef\]](#)
6. Akinola, A. On complex variable method in finite elasticity. *Appl. Math.* **2009**, *1*, 1–16. [\[CrossRef\]](#)
7. Guo, J.; Lu, Z. Line field analysis and complex variable method for solving elastic-plastic fields around an anti-plane elliptic hole. *Sci. China Phys. Mech. Astron.* **2011**, *54*, 1495–1501. [\[CrossRef\]](#)
8. Ioakimidis, N.I.; Theocaris, P.S. On a method of numerical solution of a plane elasticity problem. *Stroj. Cas.* **1978**, *29*, 448–455.
9. Strack, O.; Verruijt, A. A complex variable solution for a deforming buoyant tunnel in a heavy elastic half-plane. *Int. J. Numer. Anal. Methods Geomech.* **2002**, *26*, 1235–1252. [\[CrossRef\]](#)
10. Li, L.; Fan, T. Complex variable method for plane elasticity of icosahedral quasicrystals and elliptic notch problem. *Sci. China Ser. G: Phys. Mech. Astron.* **2008**, *51*, 773–780. [\[CrossRef\]](#)
11. Yu, J.; Guo, J.; Xing, Y. Complex variable method for an anti-plane elliptical cavity of one-dimensional hexagonal piezoelectric quasicrystals. *Chin. J. Aeronaut.* **2015**, *28*, 1287–1295. [\[CrossRef\]](#)
12. Jiao, Z.; Heblekar, T.; Wang, G.; Xu, R.; Chen, W.; Reddy, J. Analysis of plane elasticity problems using the dual mesh control domain method. *Comput. Methods Appl. Mech. Eng.* **2023**, *416*, 116342. [\[CrossRef\]](#)
13. Abdou, M. First and second fundamental problems for an elastic infinite plate with a curvilinear hole. *Alex. Eng. J.* **1994**, *33*, 227–233.
14. Abdou, M. Fundamental problems for infinite plate with a curvilinear hole having finite poles. *Appl. Math. Comput.* **2002**, *125*, 79–91. [\[CrossRef\]](#)

15. Abdou, M.; Ibrahim, E.; Basseem, M. The stress and strain components for a weakened elastic plate by two curvilinear holes in presence of heat. *Curr. Sci. Int.* **2022**, *11*, 199–216.
16. Abdou, M.; Khamis, A. On a problem of an infinite plate with a curvilinear hole having three poles and arbitrary shape. *Bull. Calcutta Math. Soc.* **2000**, *92*, 313–326.
17. Abdou, M.; Monaquel, S. Integro differential equation and fundamental problems of an infinite plate with a curvilinear hole having strong pole. *Int. J. Contemp. Math. Sci.* **2011**, *6*, 199–208.
18. Mattei, O.; Lim, M. Explicit analytic solution for the plane elastostatic problem with a rigid inclusion of arbitrary shape subject to arbitrary far-field loadings. *J. Elasticity* **2021**, *144*, 81–105. [[CrossRef](#)]
19. Alhazmi, S.E.; Abdou, M.; Basseem, M. The stresses components in position and time of weakened plate with two holes conformally mapped into a unit circle by a conformal mapping with complex constant coefficients. *AIMS Math.* **2023**, *8*, 11095–11112. [[CrossRef](#)]
20. Leonhardt, U. Optical conformal mapping. *Science* **2006**, *312*, 1777–1780. [[CrossRef](#)]
21. Trefethen, L.N. Numerical conformal mapping with rational functions. *Comput. Methods Funct. Theory* **2020**, *20*, 369–387. [[CrossRef](#)]
22. Caprini, I. Conformal mapping of the borel plane: Going beyond perturbative qcd. *Phys. Rev. D* **2020**, *102*, 054017. [[CrossRef](#)]
23. Kiosak, V.; Savchenko, A.; Gudyreva, O. On the conformal mappings of special quasi-einstein spaces. *AIP Conf. Proc.* **2019**, *2164*, 040001. [[CrossRef](#)]
24. Abdou, M.; Khar-El din, E.A. An infinite plate weakened by a hole having arbitrary shape. *J. Comput. Appl. Math.* **1994**, *56*, 341–351. [[CrossRef](#)]
25. O'Donnell, S.; Rokhlin, V. A fast algorithm for the numerical evaluation of conformal mappings. *SIAM J. Sci. Statist. Comput.* **1989**, *10*, 475–487. [[CrossRef](#)]
26. Fu, F.; Yang, X.; Zhao, P. Geometrical and physical characteristics of a class of conformal mappings. *J. Geom. Phys.* **2012**, *62*, 1467–1479. [[CrossRef](#)]
27. Ghods, M.; Faiz, J.; Gorginpour, J.; Bazrafshan, M.A.; Nøland, J.K. Equivalent magnetic network modeling of variable-reluctance fractional-slot v-shaped vernier permanent magnet machine based on numerical conformal mapping. *IEEE Trans. Transp. Electr.* **2023**, *9*, 3880–3893. [[CrossRef](#)]
28. Mukherjee, A.; Fok, P.-W. A new approach to calculating fiber fields in 2d vessel cross sections using conformal maps. *Math. Biosci. Eng.* **2023**, *20*, 3610–3623. [[CrossRef](#)]
29. Wu, L.; Zhou, Z.; Zhang, J.; Zhang, M. A numerical method for conformal mapping of closed box girder bridges and its application. *Sustainability* **2023**, *15*, 6291. [[CrossRef](#)]
30. Brociek, R.; Pleszczyński, M. Comparison of Selected Numerical Methods for Solving Integro-Differential Equations with the Cauchy Kernel. *Symmetry* **2024**, *16*, 233. [[CrossRef](#)]
31. Zhou, Y.; Lin, Y. Solving integro-differential equations with Cauchy kernel. *Appl. Math. Comput.* **2009**, *215*, 2438–2444. [[CrossRef](#)]
32. Stein, E.M.; Shakarchi, R. *Functional Analysis: Introduction to Further Topics in Analysis*; Princeton University Press: Princeton, NJ, USA, 2011. Available online: <https://books.google.com.sa/books?id=OUaU-W-dpA0C> (accessed on 22 August 2011).
33. Althubiti, S.; Mennouni, A. A Novel Projection Method for Cauchy-Type Systems of Singular Integro-Differential Equations. *Mathematics* **2022**, *10*, 2694. [[CrossRef](#)]
34. Jan, A.R.; Abdou, M.A.; Basseem, M. A Physical Phenomenon for the Fractional Nonlinear Mixed Integro-Differential Equation Using a Quadrature Nystrom Method. *Fractal Fract.* **2023**, *7*, 656. [[CrossRef](#)]
35. Assanova, A.T.; Nurmukanbet, S.N. A Solvability of a Problem for a Fredholm Integro-Differential Equation with Weakly Singular Kernel. *Lobachevskii J. Math.* **2022**, *43*, 182–191. [[CrossRef](#)]

Disclaimer/Publisher's Note: The statements, opinions and data contained in all publications are solely those of the individual author(s) and contributor(s) and not of MDPI and/or the editor(s). MDPI and/or the editor(s) disclaim responsibility for any injury to people or property resulting from any ideas, methods, instructions or products referred to in the content.